# A Realistic FDTD Numerical Modeling Framework of Ground Penetrating Radar for Landmine Detection

Iraklis Giannakis, Antonios Giannopoulos, and Craig Warren

***Abstract*—A three-dimensional (3-D) finite-difference time-domain (FDTD) algorithm is used in order to simulate ground penetrating radar (GPR) for landmine detection. Two bowtie GPR transducers are chosen for the simulations and two widely employed antipersonnel (AP) landmines, namely PMA-1 and PMN are used. The validity of the modeled antennas and landmines is tested through a comparison between numerical and laboratory measurements. The modeled AP landmines are buried in a realistically simulated soil. The geometrical characteristics of soil's inhomogeneity are modeled using fractal correlated noise, which gives rise to Gaussian semivariograms often encountered in the field. Fractals are also employed in order to simulate the roughness of the soil's surface. A frequency-dependent complex electrical permittivity model is used for the dielectric properties of the soil, which relates both the velocity and the attenuation of the electromagnetic waves with the soil's bulk density, sand particles density, clay fraction, sand fraction, and volumetric water fraction. Debye functions are employed to simulate this complex electrical permittivity. Background features like vegetation and water puddles are also included in the models and it is shown that they can affect the performance of GPR at frequencies used for landmine detection (0.5–3 GHz). It is envisaged that this modeling framework would be useful as a testbed for developing novel GPR signal processing and interpretations procedures and some preliminary results from using it in such a way are presented.**

***Index Terms*—Antennas, antipersonnel (AP) landmines, bowtie, dispersive, FDTD, fractals, GPR, GprMax, grass, modeling, roots, rough surface, vegetation, water puddles.**

## I. Introduction

NUMEROUS demining methods have been suggested over the years, from the most common and one of the first humanitarian demining methods used, the metal detector [1]–[3] to trained dogs, trained rats [4], chemical methods, nuclear methods [1], [5] and geophysical methods like acoustic/seismic [5], [6], and electrical resistivity techniques [7], [8].

Ground penetrating radar (GPR) has a wide range of applications [9] and it has been extensively used for landmine detection [10]. The ability to detect plastic landmines and the greater depth range, compared with metal detectors in dry environments with no clay or saturated soils, are some of the reasons why GPR is considered as an attractive demining method [10].

Manuscript received December 22, 2014; revised July 12, 2015; accepted July 28, 2015. Date of publication August 27, 2015; date of current version January 28, 2016. This work was supported in part by the Engineering and Physical Sciences Research Council (EPSRC) and in part by the Defence Science and Technology Laboratory (Dstl), U.K.

The authors are with the School of Engineering, Institute for Infrastructure and Environment, University of Edinburgh, Edinburgh EH9 3JL, U.K. (e-mail: I.Giannakis@ed.ac.uk; A.Giannopoulos@ed.ac.uk; C.Warren@ed.ac.uk).

Color versions of one or more of the figures in this paper are available online at http://ieeexplore.ieee.org.

Digital Object Identifier 10.1109/JSTARS.2015.2468597

A better understanding of the scattering mechanisms within the ground can help us increase the effectiveness of GPR and investigate its limitations. This can be achieved through numerical modeling that can provide insight on how the soil's characteristics can influence the overall performance of GPR. Apart from that, numerical modeling can be a practical tool for testing and comparing different antennas and processing algorithms in a wide range of environments. Furthermore, a realistic numerical model can also be employed for training purposes in machine learning based approaches. In order to address a multivariable problem like GPR demining using a machine learning approach, it will require a large number of data from a diverse set of scenarios [11]. A reasonable and viable approach to obtain a diverse, equally distributed and adequately large dataset, is through a realistic numerical modeling framework that faithfully represents the GPR forward problem.

Maxwell's equations that are the governing equations of the GPR forward problem can be numerically solved using a variety of methods, among them the finite element method, the method of moments [12], implicit finite-difference techniques (Crank–Nicolson method [13], alternative-direction implicit [14]), transmission line matrix [12], and others. The finite-difference time-domain (FDTD) method [15], [16] first introduced by Yee [19] is considered to be a very attractive choice for a number of reasons [12], [17] the most important of which are its computational efficiency and its time domain nature that particularly suits the GPR problem. We use gprMax [18] a free software, which numerically solves Maxwell's equations by using a second-order FDTD algorithm.

Numerical modeling of GPR is considered to be an alternative interpretation approach [17] and has been extensively applied to a number of GPR applications, among them are: the detection of dense nonaqueous phase liquids (DNAPL) [20], [21], the detection of geological targets like faults and caves [22], [23], for tunnel inspections [24], detecting and assessing pipes [25], in the inspection and condition assessment of bridges [26], [27], for forensic applications [28], mineral exploration [29], and airborne GPR [30]. In the case of GPR numerical modeling for landmine detection, generic types of antennas over simple targets buried in both homogenous and inhomogeneous soils have been modeled by [31]–[34]. More advanced and realistic models for both antennas and targets are employed by [35]–[37] in order to simulate single GPR traces (A-Scans), which were subsequently used as a reference in an attempt to discriminate between landmines and false alarm targets.

As stated in [10], a lot of GPR antennas were validated in ideal conditions but their performance in real complex

environments was found to differ significantly from the predicted one. Although, the probability of detection (PD) can reach near 100% and the probability of false alarm (PFA) fall to near 0.01% at simple test sites, in realistic conditions, PD can fall to 50% and PFA can reach to 10% [10]. Based on that, numerical modeling should be able to simulate and capture the behavior of GPR in realistic and appropriately complex environments and not only in clinically simplified ones. Such simplifications give rise to predictable results that cannot then be used to validate the performance of GPR in realistic conditions. Landmines can be found in a number of different environments, namely desert, jungle, urban settings, and others [10]. The proposed numerical modeling framework is here explicitly applied to rural environments. Arid as well as tropical environments can be accurately modeled using the suggested approach by simple modifications of input parameters.

One of the most challenging problems regarding the numerical modeling of GPR is how to accurately implement the dielectric properties of the soil, i.e., its frequency-dependent electrical permittivity. Simplistic models based on a constant permittivity with a conductive term cannot accurately describe the soil's behavior for frequencies employed in demining. Dielectric properties of soils are a multiparametric problem, and an analytical and completely inclusive function to describe them that has yet to be derived.

A lot of soils and rocks can be accurately simulated employing either a Cole–Cole function [38]–[40], a constant $Q$ factor [41]–[43] or the more inclusive Jonscher function that holds as a special case the constant $Q$ factor approach [44]. Both the Cole–Cole and Jonscher functions cannot be directly implemented into an FDTD code. Approximations to these functions with multi-Debye relaxations [45]–[47] are the most usual approach for implementing these type of dielectric properties into FDTD. Numerically evaluated fractional derivatives [48] and Pade approximations [49] have also been suggested for implementing complex dielectric properties. Multi-Debye expansions, however, are more computationally efficient because it is straightforward to choose the frequency range in which the approximation will take place. By reducing the frequency range, the number of Debye poles needed for an adequate approximation is decreased, which subsequently results in an overall decrease of the computational requirements.

A number of authors have used multi-Debye functions in an effort to simulate simple homogenous soils [50]–[55]. Although, these approaches simulate the dielectric properties of the specific soils correctly, the use of homogenous models is still an oversimplification. A more inclusive approach is needed if different types of soils are to be modeled. In the present work, we use the semiempirical model initially suggested by [56] and later modified by [57] and [58]. This semiempirical model relates the dielectric properties of the soil to its bulk density, sand particles density, soil fraction, clay fraction, and water volumetric fraction. The semiempirical model resembles the Cole–Cole relaxation and can be easily approximated by a multi-Debye expansion. Using this approach, a wide range of diverse soils can be incorporated into the model, as well as complex media with realistic statistical variation of properties like water fraction, clay fraction, and so on.

Rough surface can have a significant affect to the overall performance of GPR [9], [59]. Thus, a realistic numerical model should include a representation of the roughness of soil's surface. Fractals can express the earths topography with representative detail [60] for a wide range of scales. Therefore, fractal correlated noise [61] was chosen to describe the stochastic nature of the soil's topography. Fractal correlated noise is also employed in an effort to describe the soil's inhomogeneity. There is an evidence in the literature [62]–[65], which supports the premise that for the scales used in the simulations presented here, fractals give rise to semivariograms often encountered in real soils.

Vegetation is a very important feature considering the GPR frequency range employed in demining and should not be neglected neither just simply defined. Both grass and roots are realistically incorporated into the suggested modeling scheme and simulated results indicate that they could have an effect on the overall performance of GPR. A novel algorithm is proposed that generates the geometry of both grass and roots with representative detail. The suggested algorithm creates the geometry of vegetation automatically having as its inputs statistical characteristics like grass distribution, maximum height of grass blades, maximum depth of roots, standard deviation of grass height, standard deviation of the maximum depth of roots, and properties related to the shape of the grass and roots. Regarding the dielectric properties of vegetation, a multi-Debye expansion is used to approximate the function suggested in [66] and [67]. The latter relates the complex electrical permittivity of vegetation with its water weight based fraction. Water puddles are also incorporated into the numerical scheme in an attempt to simulate more humid environments.

Numerical modeling has been widely used for designing and optimizing antennas. From complex antennas [68], [69] to more common designs are bowties [70]–[72], dipoles [73], vee dipoles [74], spiral [75], and horn antennas [76]. In addition, FDTD has been successfully employed to model generic types of antennas based on generic designs used in commercial ones [77]–[79]. In the present work, we use models of generic bowtie high-frequency GPR transducers based on the geometrical characteristics obtained from commercially available antennas like the GSSI 1.5 GHz and the MALA 1.2 GHz as presented in [77]. Both of these GPR antennas are designed mostly for engineering applications because of their high-frequency range and their availability for simple testing, which have been chosen to illustrate the effectiveness of the proposed modeling framework for landmine detection.

The targets used in the simulations are detailed representations of the AP landmines PMA-1 and PMN. Dummy landmines have been used to obtain their geometrical characteristics. The dielectric properties of the AP landmines have been chosen from an iterative process of matching numerical and laboratory measurements of scattered electromagnetic fields in free space.

## II. Soil Modeling

Soil modeling consists of two parts: the first part addresses the dielectric properties of the soil and the second deals with the

soil's geometrical characteristics, i.e., the soil's inhomogeneity and rough surface.

### A. Dielectric Properties of the Soil

In this work, a semiempirical model—initially suggested in [56]—is used to describe the dielectric properties of the soil. This semiempirical model relates the soil's relative permittivity to simply determined properties, namely bulk density, sand particles density, sand fraction, clay fraction, and water volumetric fraction. Using this approach, a realistic soil with a stochastic distribution of the aforementioned parameters can be modeled.

The semiempirical model was originally suggested for the frequency range of 1.4–18 GHz [56]. Used in that form and for frequencies below 1.4 GHz, it underestimates $\epsilon'$ and overestimates $\epsilon''$ [57], [58]. Therefore, a modification was introduced in [57] and [58] for the frequency range of 0.3–1.3 GHz. In our proposed modeling framework, the dielectric mixing model is chosen based on the central frequency of the excitation pulse. If the central frequency is below 1.4 GHz, the model for 0.3–1.3 GHz [57], [58] is used otherwise the model suggested for 1.4–18 GHz [56] is employed. Both models are described by (1)–(9), where $\epsilon_m = \epsilon' - j\epsilon''$ is the complex electrical permittivity of the defined medium, $j$ is the imaginary unit $\left(j = \sqrt{-1}\right)$, $m_u$ is the water volumetric fraction, $\rho_s$ is the sand particles density $(\mathrm{g/cm^3})$, $\rho_b$ is the bulk density of the soil $(\mathrm{g/cm^3})$, $\epsilon_s$ is the relative permittivity of the sand particles, $a = 0.65$ is an experimentally derived constant, and $S$ and $C$ are the sand and clay fractions, respectively. The complex dipolar relaxation of water is described by (7), where $t_{0,w} = 9.23$ ps is the relaxation time of the water, $\epsilon_{w,s} = 80.1$ and $\epsilon_{w,\infty} = 4.9$ are the relative electrical permittivity of the water for zero and infinity frequencies, respectively [57]. The term $\sigma_f$ is a linearly proportional term to the conductivity $\sigma$

$$\epsilon'_{(1.4-18\,\mathrm{GHz})} = \epsilon_0 \left(1 + \frac{\rho_b}{\rho_s}(\epsilon_s^a - 1) + m_u^{\beta'} \epsilon_w'^a - m_u\right)^{1/a} \tag{1}$$

$$\epsilon'_{(0.3-1.3\,\mathrm{GHz})} = 1.15\epsilon'_{(1.4-18\,\mathrm{GHz})} - 0.68 \tag{2}$$

$$\epsilon'' = \epsilon_0 m_u^{\frac{\beta''}{a}} \left(\frac{\sigma_f}{\omega\epsilon_0}\frac{(\rho_s - \rho_b)}{\rho_s m_u} - \epsilon''_w\right) \tag{3}$$

$$\epsilon_s = (1.01 + 0.44\rho_s)^2 - 0.062 \tag{4}$$

$$\beta' = 1.2748 - 0.519S - 0.152C \tag{5}$$

$$\beta'' = 1.33797 - 0.603S - 0.166C \tag{6}$$

$$\epsilon_w = \epsilon_{w,\infty} + \frac{\epsilon_{w,s} - \epsilon_{w,\infty}}{1 + j\omega t_{0,w}} \tag{7}$$

$$\sigma_{f(1.4-18\,\mathrm{GHz})} = -1.645 + 1.939\rho_b - 2.25622S + 1.594C \tag{8}$$

$$\sigma_{f(0.3-1.3\,\mathrm{GHz})} = 0.0467 + 0.2204\rho_b - 0.411S + 0.6614C. \tag{9}$$

Fig. 1 shows the relative electrical permittivity (using the model suggested for 0.3–1.3 GHz) for $\rho_s = 2.66\ \mathrm{g/cm^3}$, $\rho_b = 2\ \mathrm{g/cm^3}$, $S = 0.1$, $C = 0.9$, and for $m_u = 0.05{-}0.25$ with a step of 0.05. Fig. 2 is similar to Fig. 1 with $S = 0.9$ and $C = 0.1$. It is evident that the real part of the electrical permittivity is practically constant over the frequency range of interest for landmine detection (0.5–3 GHz) and it increases when the volumetric water fraction is increased. Increasing the clay fraction results in the decrease of the real part of the electrical permittivity, i.e., increasing the velocity of the EM waves.

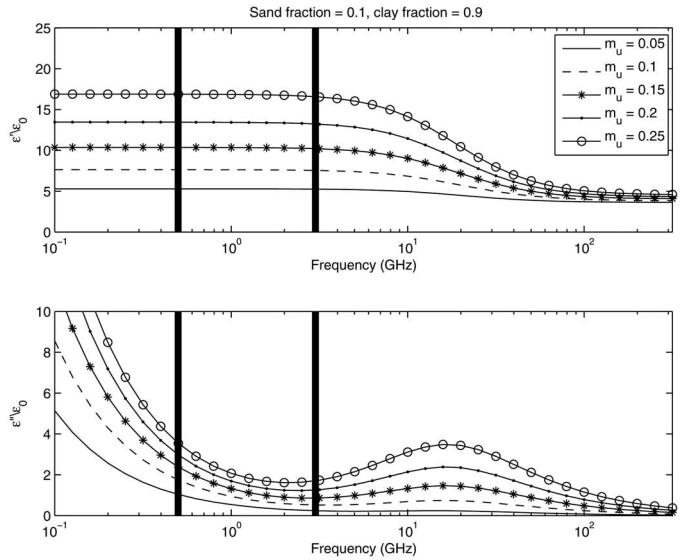


Fig. 1. Relative electrical permittivity for $\rho_s = 2.66\ \mathrm{g/cm^3}$, $\rho_b = 2\ \mathrm{g/cm^3}$, $S = 0.1$, $C = 0.9$ and for $m_u = 0.05{-}0.25$ with step 0.05. The frequency range of GPR for landmine detection is denoted between the bold lines.

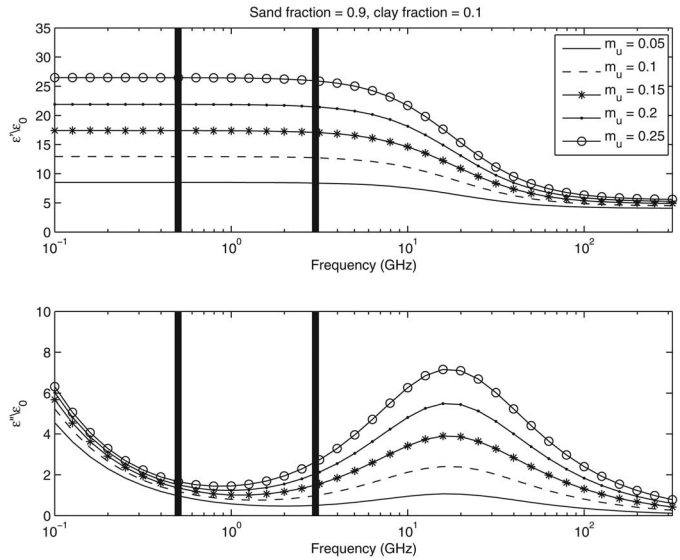


Fig. 2. Similar to Fig. 1 using $S = 0.1$ and $C = 0.9$.

At first that seems not to be in good agreement with the general experience, which expects low velocities in clay environments. This apparent peculiar result could be easily explained from the fact that clay environments (due to the high porosity of clays) have usually significant water content that results in the decrease of their overall velocity. However, dry clay on the other hand has equal or even smaller real part of relative permittivity compared with dry sand [9]. Furthermore, due to the

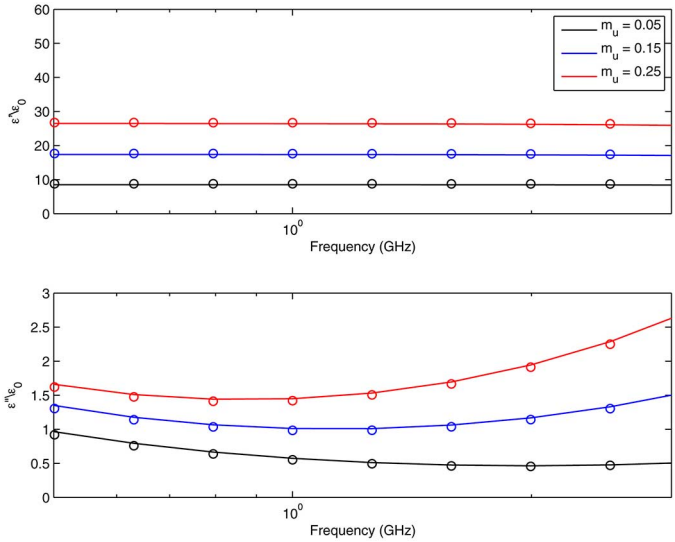


Fig. 3. Exact (lines) and the single pole Debye approximations (dots) of the relative electrical permittivity for the frequency range of interest (0.5–3 GHz). The properties of the soil are $\rho_s = 2.66$ g/cm$^3$, $\rho_b = 2$ g/cm$^3$, $S = 0.9$, $C = 0.1$, and for $m_u = 0.05{-}0.25$ with step equals 0.1.

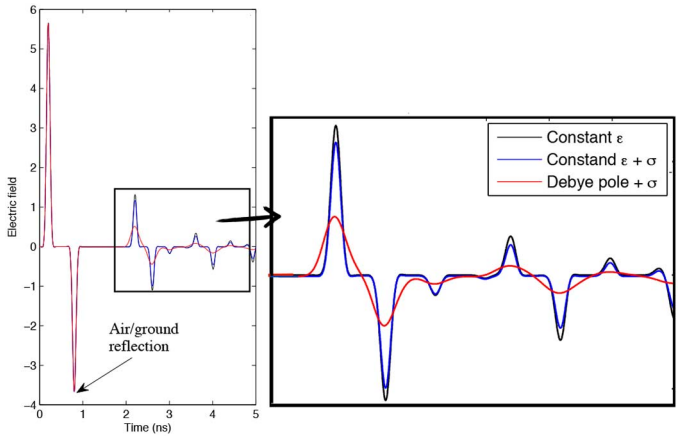


Fig. 4. Resulting scattering fields for a plane wave propagating in a four layer medium (air–soil–plastic–soil). Three different approaches are used for both soils to define their dielectric properties. With black, only a constant electrical permittivity is used. With blue, a constant electrical permittivity plus a conductive term is employed and with red, the full model (i.e., a Debye pole with a conductive term) is implemented.

high porosity of clays, dry clays could have a large fraction of air that adds to the overall increase of their velocity.

The imaginary part of the electrical permittivity consists of two parts: one related to the conductive term and another related to the Debye relaxation due to the water content (3). Increasing the water volumetric fraction results in an increase of the imaginary part (i.e., the attenuation) and also increases the contribution of the Debye relaxation. Increasing the clay fraction makes the electromagnetic losses to be primarily related to the conductive term and decreases the effects of the Debye relaxation at the frequency range used for landmine detection (0.5–3 GHz).

As the the semiempirical model cannot be directly implemented into FDTD, a particle swarm optimization (PSO) [80] has been used to approximate both the real and the imaginary part of the dielectric model explained in (1)–(9) with a conductive term plus a multipole Debye function (10)

$$\epsilon_m \approx \epsilon_\infty + \frac{\sigma}{j\omega} + \sum_{p=1}^{N} \frac{\Delta\epsilon_p}{1 + j\omega t_{0,p}} \tag{10}$$

where $N$ is the number of the Debye poles and $\Delta\epsilon_p = \epsilon_{p,s} - \epsilon_{p,\infty}$.

In order for FDTD to be stable, $\Delta\epsilon_p$ must be positive and $\epsilon_\infty$ must be greater than $\epsilon_0$ [46]. By increasing the number of Debye poles, the approximation becomes more accurate but for each extra Debye pole three additional memory variables are needed to be stored for each FDTD cell with dispersive dielectric properties. A balance between accuracy of the fit and computational cost must be achieved in order for the simulations to be both accurate and practical. For the frequency range of interest, a single Debye pole has been found to be an adequate approximation as it is shown at Fig. 3. Accurate approximations for wider range of frequencies require more Debye poles to be used subsequently increasing the computational requirements.

In order to illustrate the importance of implementing a realistic loss mechanism into the modeling scheme, a numerical experiment was performed using a simple one-dimensional (1-D) FDTD model. The model consists of four layers, namely air, soil, plastic, and soil. The excitation is a Gaussian-modulated sinusoidal pulse with central frequency 2 GHz. The relative electrical permittivity of plastic was chosen to be $\epsilon_p = 3$. Three different scenarios were tested. 1) A simple constant electrical permittivity is implemented without any losses. 2) A conductive term is added. 3) A Debye pole plus a conductive term are employed. The soil's properties are $\rho_s = 2.66$ g/cm$^3$, $\rho_b = 2$ g/cm$^3$, $S = 0.9$, $C = 0.1$, and $m_u = 0.2$. Fig. 4 illustrates that the full Debye model with a conductive term apart from further decreasing the amplitude of the pulse, it also lowers the central frequency of the scattering field that subsequently reduces the ability of the pulse to resolve small targets. Electromagnetic losses can have a significant effect to the overall signal to noise ratio as well as to the shape of the target's scattering field. From the above example, it is evident that simple definitions of the loss mechanisms within the soil can result in a potential overestimation of GPR's performance. Thus, an accurate implementation of the dielectric properties is essential for a realistic numerical modeling scheme, which aims to be used as a testbed for different processing algorithms or as a training platform for machine learning approaches.

### B. Soil's Geometrical Characteristics

Fractals are scale-invariant functions, which can express the earths topography for a wide range of scales with sufficient detail [60]. This is the reason why fractals were chosen in this work to represent the soil's topography. Fractals can be generated by the convolution of Gaussian noise with the inverse Fourier transform of $1/k^b$, where $k$ is the wavenumber and $b$ is a constant related with the fractal dimension [61]. Fig. 5

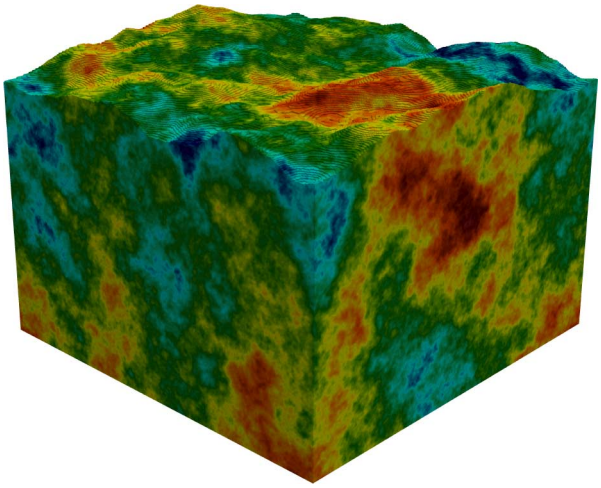

Fig. 5. Stochastic distribution of an arbitrarily chosen property of the soil (e.g., water volumetric fraction, clay fraction, and sand density). The rough surface as well as the soil's property distribution are created using a fractal-based approach.

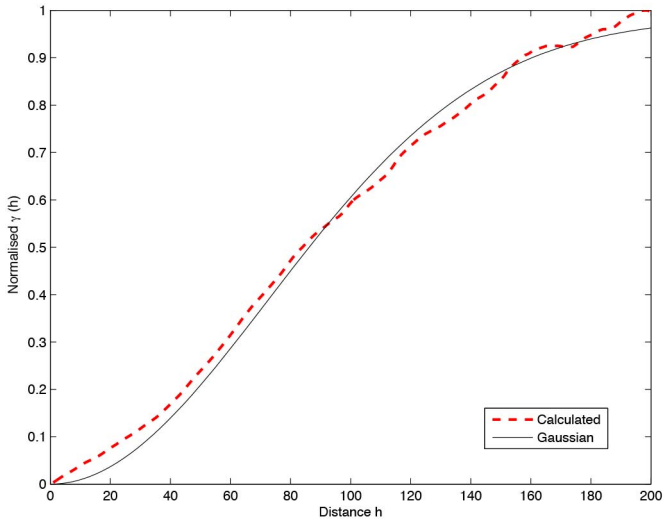


Fig. 6. Calculated semivariogram (dots) and simulated Gaussian semivariogram (solid line) of the arbitrarily chosen property of the soil shown in Fig. 5. The distance $h$ is unit-less and represents the pixels in Fig. 5.

illustrates the resulting rough surface using fractal correlated noise. Increasing the fractal dimension results to the increase of the roughness of the soil's surface. The semivariogram (11) is a geostatistical tool used to describe correlation lengths and it is an attractive approach to describe the stochastic nature of soil's properties

$$\gamma(h) = \frac{1}{2V}\sum_{i=1}^{V}|z(i+h) - z(i)|^2 \tag{11}$$

where $h$ is the lag distance, $z$ is the investigated property (water fraction, clay fraction, bulk density, etc.), and $V$ is the number of the observations for each lag length ($h$). Soil's properties usually follow exponential, spherical or Gaussian semivariograms [62]–[64]. In this work, a fractal correlated noise [61] is used to describe the stochastic distribution of the soil's properties. This approach is chosen because as it is stated in [81] and [82], soil-related environmental properties frequently obey fractal laws. Furthermore, as it is shown in Fig. 6, the distribution of an arbitrarily property using three-dimensional (3-D) fractals results in Gaussian semivariograms for the scales used for AP landmine detection.

Fig. 5 illustrates an example of a stochastic soil's property distribution (e.g., water volumetric fraction, clay fraction, sand density etc.) and rough surface created using fractal correlated noise. Fig. 6 shows the simulated Gaussian and the calculated semivariogram for the model shown in Fig. 5. A Gaussian semivariogram can simulate the calculated one with sufficiently accuracy , which is an indicator of the reliability of the modeled soil. Soil's inhomogeneity affect GPR's performance by decreasing the signal to noise ratio and by increasing the false alarm rate. A numerical scheme aiming to facilitate the development of processes to address such problems (through processing validation, antenna design, machine learning etc.) must be able to accurately simulate such negative effects. Modeling soil's inhomogeneity by using simple deterministic shapes and unrealistic property distributions may lead to data that are not suitable for machine learning purposes neither for evaluation of processing techniques.

## III. Vegetation

AP landmines are shallow buried targets, typically no more than 10 cm, and their diameter is usually 10–20 cm [3]. Therefore, in order for AP landmines to be detectable high-frequency antennas are employed (0.5–3 GHz). The use of high-frequency antennas leads to an increased sensitivity to small scale features such as grass and roots. In order to investigate the effects of vegetation to AP landmine detection using GPR, we propose an algorithm that models the geometrical characteristics of vegetation using statistical properties. The steps of the proposed algorithm are as follows.

1) A two-dimensional (2-D) fractal is created and the summation of the fractal values is constrained to be equal to one. Each fractal value represents the probability of a blade of grass to exist in the corresponding coordinates of this value $(x_c, y_c)$.
2) For each blade of grass, a maximum height is picked based on a Gaussian distribution.
3) The parametric equations of each blade of grass are (for $0 < t <$maximum height)

$$x = x_c + s_x\left(\frac{t}{b_x}\right)^2 \tag{12}$$

$$y = y_c + s_y\left(\frac{t}{b_y}\right)^2 \tag{13}$$

$$z = t \tag{14}$$

where $s_x$ and $s_y$ can be 1 or $-1$ and they are randomly chosen. The constants $b_x$ and $b_y$ are random numbers based on a Gaussian distribution.
4) For each blade of grass, a root is placed in the same coordinates $(x_c, y_c)$ and a maximum depth for the root is picked based on a Gaussian distribution.

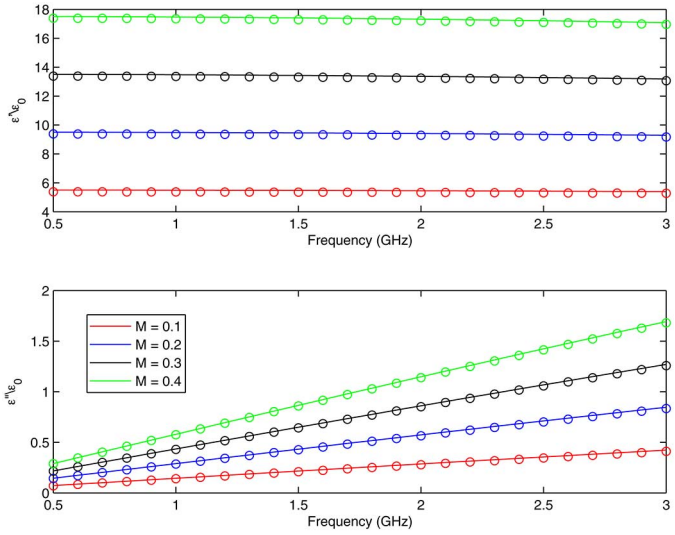


Fig. 7. Debye approximations (dots) compared with the analytic (lines) relative electrical permittivity of vegetation (18) for water weight fraction $M = 0.1-0.4$ with step 0.1.

3) The function, which describes the geometry of the roots, is a random walk in $x$ and $y$ coordinates as the depth increases linearly

$$x_{i+1} = x_i + R_x \tag{15}$$
$$y_{i+1} = y_i + R_y \tag{16}$$
$$z_{i+1} = z_i - \Delta z \tag{17}$$

where both $R_x$ and $R_y$ are random variables based on a Gaussian distribution and $\Delta z$ is the depth discretization step. The iterative procedure described in (15)–(17) continues until $z$ reaches the maximum depth of the root.

Dielectric models of plants like leaves of corn [83], stalks, trunks [84], [85] alfalfa [86], conifer trees [87], etc., have been reported in the literature. In the present work, the formula (18) suggested in [66] and [67] is employed in an effort to describe the dielectric properties of vegetation

$$\epsilon_g' - j\epsilon_g'' = 1.5 + \left(\frac{\epsilon_w'}{2} - j\frac{\epsilon_w''}{3}\right) M \tag{18}$$

where $\epsilon_w'$ is the real part of the electrical permittivity of the water, $\epsilon_w''$ is the imaginary part of the permittivity of the water, $j$ is the imaginary unit ($j = \sqrt{-1}$), and $M$ is the water content based on a weight basis [67].

The main drawback of this model is that it is validated only to a single frequency of 8.5 GHz. Extending (18) to the wider frequency range of interest (0.5–3 GHz) results in an electrical permittivity that has a constant real part and an imaginary part, which increases linearly with the frequency. This seems reasonable, but as it is reported in [67], the extension of this model to other frequencies should be checked experimentally.

Similar to soil modeling, a PSO is used [80] to simulate (18) with a multi-Debye function (10). For the frequency range of interest, a single Debye pole can sufficiently approximate (18) for different water weight-based fractions ($M$) as it is shown in Fig. 7.

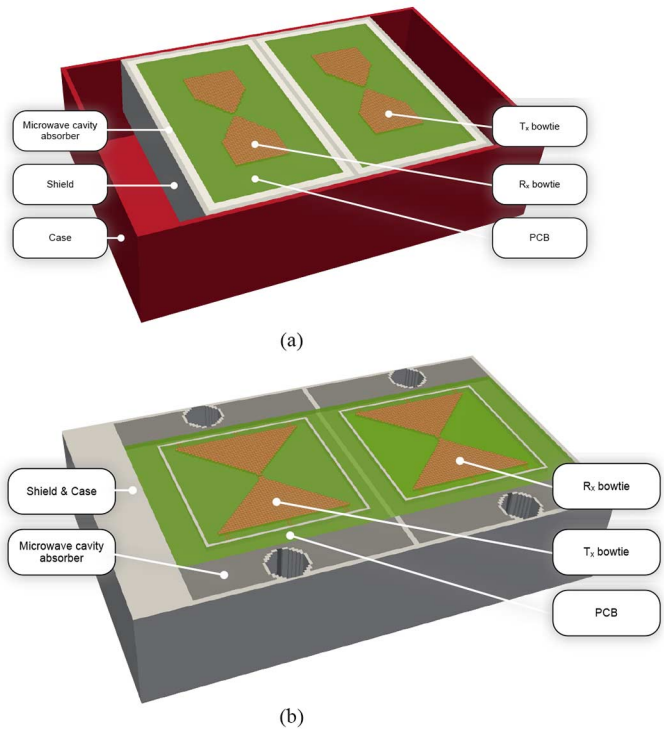


Fig. 8. Modeled antennas. (a) 1.5 GHz. (b) 1.2 GHz [77].

## IV. Antennas and Landmines

The GPR transducers used in this work are models of bowtie antennas based on the geometrical characteristics of commercial GPR antennas, namely the GSSI 1.5 GHz and the MALA 1.2 GHz [77], [78] (see Fig. 8). Using realistic models of GPR antennas is a reliable way to illustrate the capabilities of the proposed numerical scheme. When information is provided by manufacturers and antenna developers complex antennas can be accurately modeled and directly evaluated in realistic scenarios. Furthermore, bowtie antennas have been successfully applied for landmine detection [8] and have been also employed in previous published numerical schemes focusing on landmine detection [35], [37].

The targets employed in the simulations are the AP landmines PMA-1 and PMN. Both of them are widely used and frequently found in minefields [88], [89]. PMA-1 is a blast AP landmine with minimum metal content. It was manufactured in former Yugoslavia and was used in the Balkan area [89]. Because of the metal fuse inside PMA-1, it is possible to be detected with metal detector, but there are also reported types of PMA-1 with plastic fuses. PMA-1 has 200 g of high explosive content (TNT). The dimensions of PMA-1 are: height 30 mm, length 140 mm, width 65 mm. Fig. 9 illustrates the modeled AP landmine. The discretization step used for the model is $\Delta x = \Delta y = \Delta z = 1$ mm. Larger discretization step can be applied in a straightforward manner with a simple interpolation. PMN is one of the oldest landmines that are still in use. It is manufactured in Russia and it is one of the most widely employed landmines [88]. Similar to PMA-1, PMN has a large amount of high explosive (240 g TNT). PMN is a palm shaped cylindrical blast AP landmine. It has a minimum metal

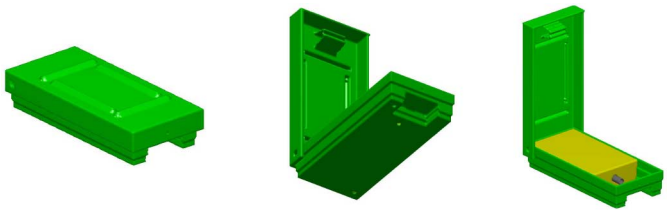

Fig. 9. Modeled AP landmine PMA-1. Green is plastic ($\epsilon = 2.5$), gray is perfect conductor (PEC), and yellow is rubber ($\epsilon = 6$).

Fig. 10. Modeled AP landmine PMN. The adapted side parts of the landmine are shown at the right of the image. The black top of the AP landmine is rubber ($\epsilon = 6$), the black pieces on the adapted parts is bakelite ($\epsilon = 3.5$), shiny gray is perfect conductor (PEC), blue is plastic ($\epsilon = 3$), the gray parts of the landmine are also bakelite ($\epsilon = 3.5$), and the inside of the landmine is rubber ($\epsilon = 6$).

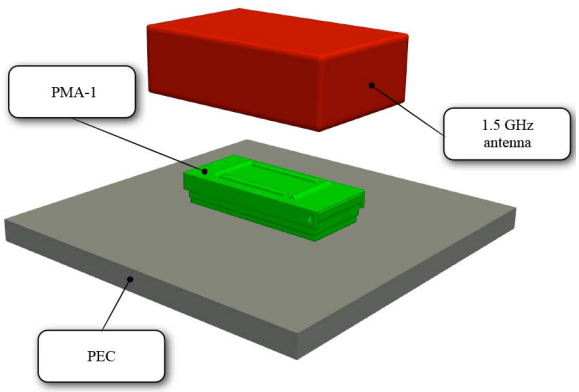


Fig. 11. 1.5-GHz antenna (red box) operates 10 cm above a PEC on which the PMA-1 is placed. The same experiment was also executed using the PMN.

content, which can make the PMN detectable with metal detectors. The dimensions of PMN are: height 50 mm and diameter 115 mm. Fig. 10 shows the modeled PMN, the discretization of the model is $\Delta x = \Delta y = \Delta z = 1$ mm. The dielectric properties of the modeled AP landmines are chosen such as the numerical and the real A-Scans from the experiment shown in Fig. 11 were in good agreement. During the experiment, both of the AP landmines were placed over a perfect electrical conductor (PEC) and the antenna was positioned at 10 cm above the PEC. The antenna unit chosen for the experiment was the 1.5-GHz antenna. Fig. 12 illustrates that the numerical and the real normalized A-Scans are in good agreement, which indicates the accuracy of the modeled AP landmines.

## V. Simulation Results

For the simulations, we used gprMax [18] a free software, which solves Maxwell's equations using a second-order accurate FDTD method [19]. In all of the models, the discretization step was set to $\Delta x = \Delta y = \Delta z = 1$ mm and the time step was

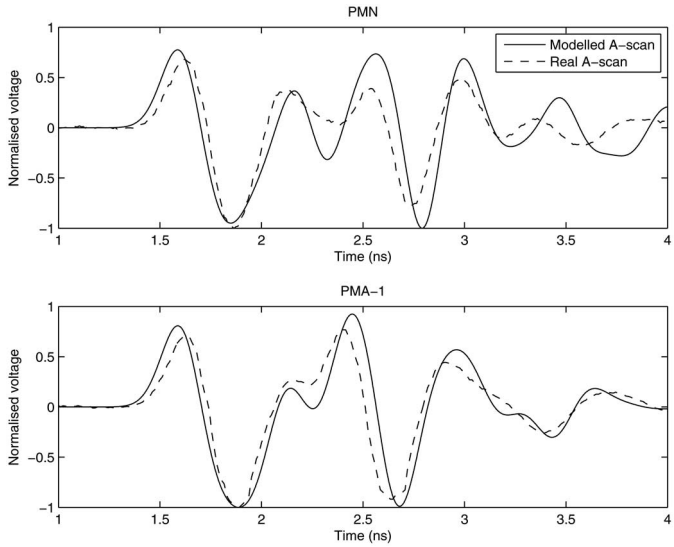


Fig. 12. Numerical and real normalized A-Scans for the experiment described in Fig. 11 using both PMA-1 and PMN.

equal to the Courant limit for the 3-D FDTD scheme ($\Delta t = 1.925$ ps) [15]. A small discretization step increases the computational cost but it is essential to model the geometry of soil, targets, vegetation, and antennas with very good resolution. In addition, a small discretization step tackles the unnatural dispersion, which occurs to small wavelengths due to numerical errors inherent in the FDTD [15]. Regarding the absorbing boundary conditions, a perfectly matched layer (PML) [15], [90] with 10 cells thickness is applied to all the simulations.

The computational requirements are related to the model's size, its dielectric properties and the maximum number of iterations required for a given GPR time window. Dispersive soils have increased computational requirements compared to nondispersive media. In that context, a $1000 \times 400 \times 300$ (cells) model consisted entirely of dispersive media needs approximately 8-GB of random-access memory (RAM). Using six processors and 12-GB of RAM, the computation time for such a model was approximately 2 h per trace for 2500 iterations.

The computational resources required for these kinds of modeling problems are more than what a conventional computer can offer if results are to be obtained in reasonable time. To overcome this obstacle, we have employed ECDF [91], the cluster computer of the University of Edinburgh. A parallelized version of gprMax has allowed us to compute complete B-Scans in the same time that was needed for computing a single A-Scan on a single workstation.

### A. Vegetation

In the first example, we examine how vegetation affects landmine detection using GPR. The model's dimensions are $1000 \times 250 \times 450$ mm, the surface is relatively smooth, the soil's properties are $\rho_s = 2.66\ \mathrm{g/cm^3}$, $\rho_b = 2\ \mathrm{g/cm^3}$, $C = 0.5$, $S = 0.5$, and the water volumetric fraction varies stochastically from $m_u = 0$ to 0.25. The height of grass blades varies from

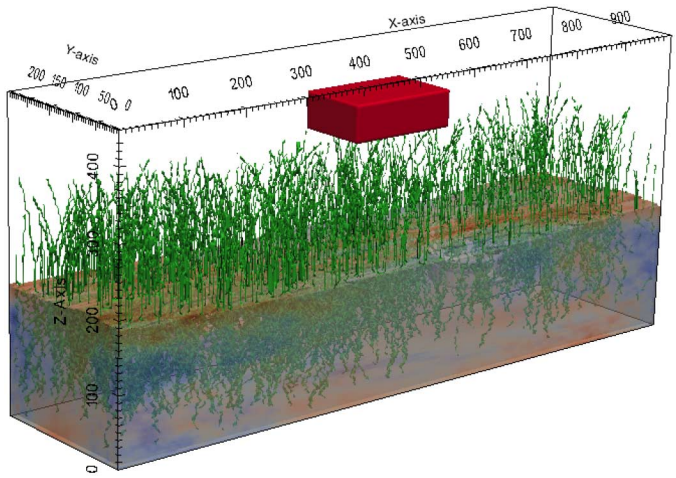


Fig. 13. AP landmines PMN and PMA-1 buried in a soil with stochastic varied water volumetric fraction from $m_u = 0-0.25$. Red color depicts the dry areas while with blue colors saturated areas are illustrated. The red box is the antenna unit. The axis are in millimeter.

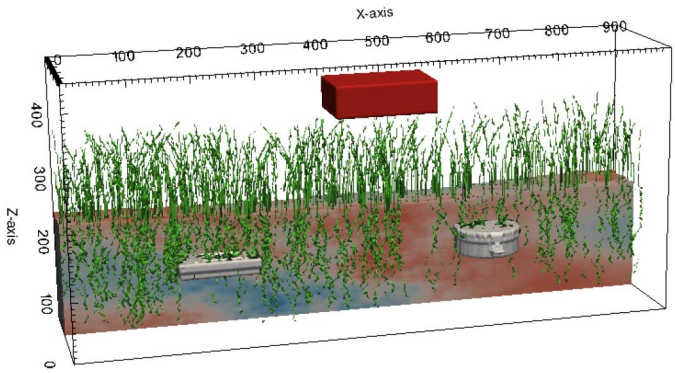


Fig. 14. Slice parallel to the tomography line of the model shown in Fig. 13.

20 to 130 mm and the roots from 20 to 200 mm. Three different scenarios were tested with both antenna models. In the first scenario, the water weight-based fraction of the vegetation is equal to $M = 0.4$ (saturated grass and roots). In the second scenario, the water weight-based fraction is $M = 0.1$ (dry grass and roots) and in the third scenario, there is no vegetation. Figs. 13 and 14 illustrate the geometry of the model. The height of the antenna unit is approximately 160 mm above the ground and 20 mm above the grass. The depth of both landmines is approximately $50-70$ mm. The B-Scan is taken place along the $x$-axis. The moving step of the antenna is 6 mm, which results in a B-Scan consisted of 132 traces. To all the simulations presented in this section a quadratic gain and subsequently a singular value decomposition (SVD) [92], having three dominant eigenvalues filtered out, are applied to the raw data. After removing the ground clutter and the ringing noise, the energy of each trace is calculated by (19)

$$P(x) = \int_0^\infty E_y(x,t)^2 dt. \tag{19}$$

Fig. 15 presents the B-Scans and normalized energy plots for the present model (see Figs. 13 and 14) using the 1.5-GHz antenna. In the absence of vegetation, both AP landmines can

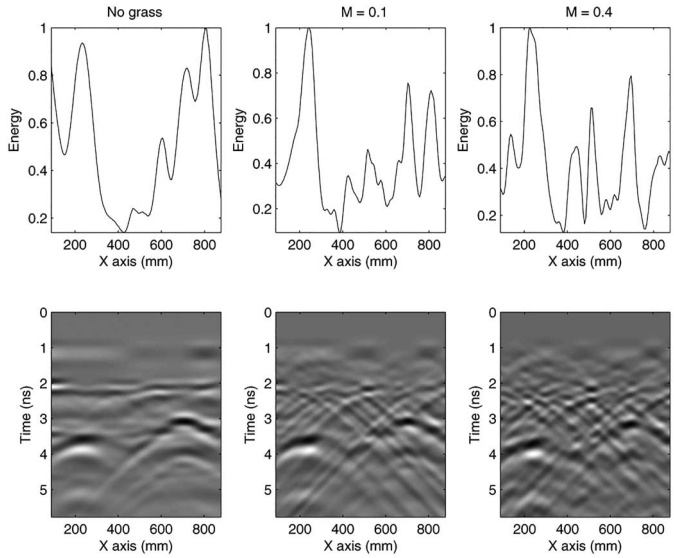


Fig. 15. B-Scans and normalized energies of the model shown in Fig. 13 with and without vegetation. The vegetation's water weight-based fraction equals $M = 0.1$ and $M = 0.4$. The 1.5-GHz antenna is used in the simulations. A quadratic gain and subsequently a singular value decomposition (three dominant eigenvalues are filtered out) are applied to the raw data. The $X$-axis corresponds to the center of the antenna unit in each trace.

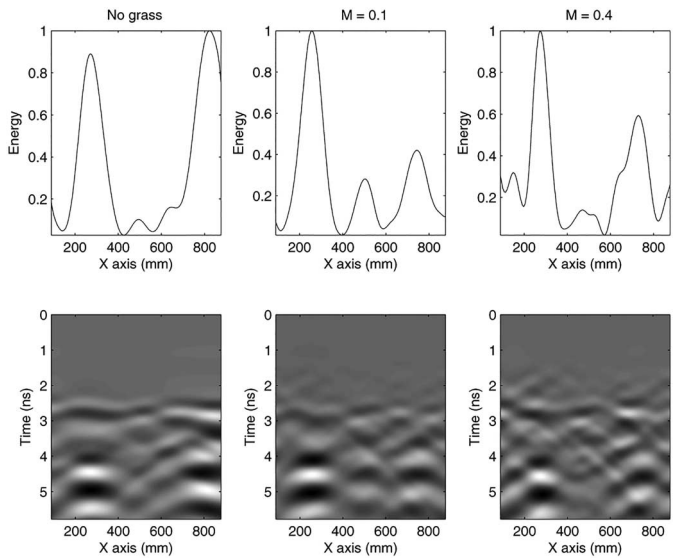


Fig. 16. Similar to Fig. 15 using the 1.2-GHz antenna.

be reliably detected from the B-Scans and the energy plots. When vegetation is present and as the water weight-based fraction increases, B-Scans as well as energy plots become noisy and more difficult to interpret. This is due to the high-frequency content of the antenna (1.5 GHz), which results in an increased sensitivity to features such as vegetation. Using a higher-frequency antenna will further increase this problem. Using the 1.2-GHz antenna, due to the slightly lower-frequency content of the pulse, the effects of vegetation are not as dominant. However, vegetation can result in false alarms as it is shown in Fig. 16 for $M = 0.1$. This study shows that the simulated vegetation is not a negligible feature and it can potentially affect the performance of GPR for the frequency range used for

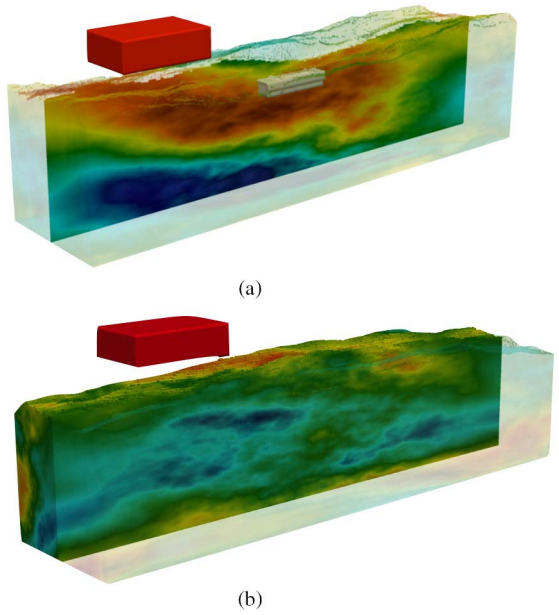


Fig. 17. (a) Buried AP landmine PMA-1 in a stochastically varied soil. (b) No landmine is buried in order to get an insight on the resulting clutter. The properties of the soil (for both cases) are $\rho_s = 2.66\ \mathrm{g/cm^3}$, $\rho_b = 1.5\ \mathrm{g/cm^3}$, $C = 0.5$, $S = 0.5$, and water volumetric fraction, which varies from $m_w = 0{-}0.25$. The antenna unit used is the 1.5 GHz.

landmine detection. Nonetheless, Figs. 15 and 16 illustrate that GPR has the potential to be effective in grassy environments in which vegetation removal is not trivial due to tripwires that might be present [3].

### *B. Soil's Inhomogeneity*

Apart from vegetation, more frequently encountered features like soil's inhomogeneity can also result in false alarms and mask the landmine's scattering field [93]. Most of the numerical modeling done so far, as well as some real field experiments took place in simplified/clinical settings. This overestimates the performance of GPR and gives often a false impression regarding its abilities and its limitations. The dimensions of the models in this section are $1000 \times 250 \times 350$. The properties of the soil are $\rho_s = 2.66\ \mathrm{g/cm^3}$, $\rho_b = 1.5\ \mathrm{g/cm^3}$, $C = 0.5$, $S = 0.5$, and the water volumetric fraction varies from $m_w = 0$ to $0.25$. The model antenna used was the 1.5 GHz and it is placed relatively close to the ground. Two cases are presented. 1) the AP landmine PMA-1 is placed at the center of the model at approximately 40 mm depth from the surface. 2) No landmines are present in an effort to put the emphasis on the level of the resulting clutter (see Fig. 17). Fig. 18 presents the resulting B-Scans using the 1.5-GHz antenna. A quadratic gain is initially applied to the raw data. Subsequently, three different processing methods were used: 1) a high pass filter; 2) an adaptive scaled and shifted (ASaS) method [94], [95]; and 3) an SVD filtering out three dominant eigenvalues. It is evident that the landmine's signature is masked from the ground clutter (low signal-to-noise ratio). In addition, the soil's inhomogeneity can give rise to false alarms as a result of the presence of inhomogeneous clusters in the ground. From the above, it is

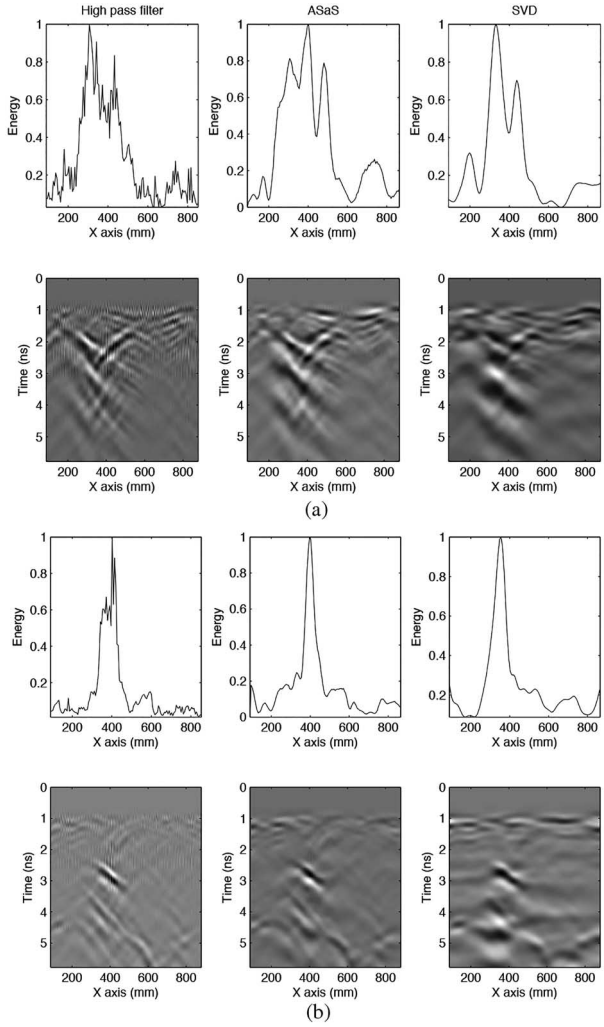


Fig. 18. B-Scans using the 1.5-GHz antenna for the models illustrated in Fig. 17. A high pass filter, ASaS, and an SVD (three dominant eigenvalues are filtered out) are applied subject to a quadratic gain.

concluded that soil's inhomogeneity is an essential feature for a realistic and useful numerical modeling framework aiming to reliably assist in evaluating a GPR's performance. Realistic and complex B-Scans from high clutter environments can provide a challenging testbed for evaluating as well as comparing different processing approaches and antenna designs.

### *C. Targets*

Different targets give rise to different scattered signatures. For high-frequency problems like GPR for AP landmine detection, detailed modeling of the targets of interest is a basic requirement if, i.e., the numerical scheme is to be used as a training platform for machine learning. In the present section, the importance of accurate models of landmines is illustrated. The two AP landmines, PMN and PMA-1, are buried in the same stochastically varied soil (see Fig. 19) in an effort to illustrate the different resulting B-Scans. The dimensions of the models in this section are $1000 \times 250 \times 350$. The rough surface as well as the soil's inhomogeneity are modeled using fractal correlated noise. The properties of the soil are $\rho_s =$

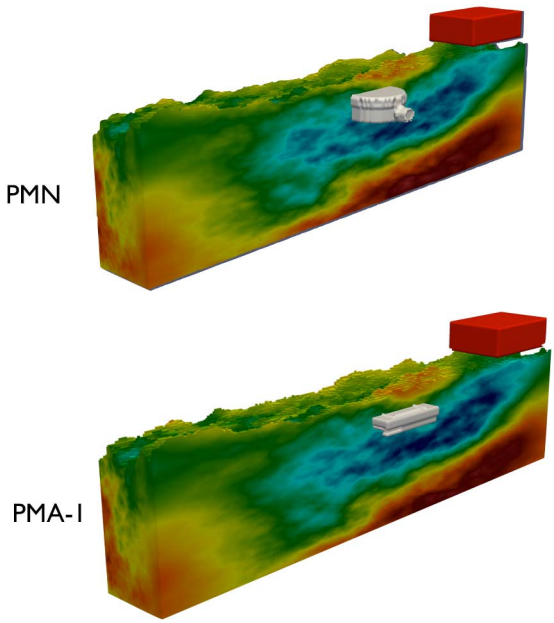


Fig. 19. Buried AP landmines PMA-1 and PMN in a stochastically varied soil. The properties of the soil are $\rho_s = 2.66$ g/cm$^3$, $\rho_b = 1.5$ g/cm$^3$, $C = 0.5$, $S = 0.5$, and water volumetric fraction, which varies from $m_w = 0{-}0.25$. The antenna unit used is the 1.5 GHz.

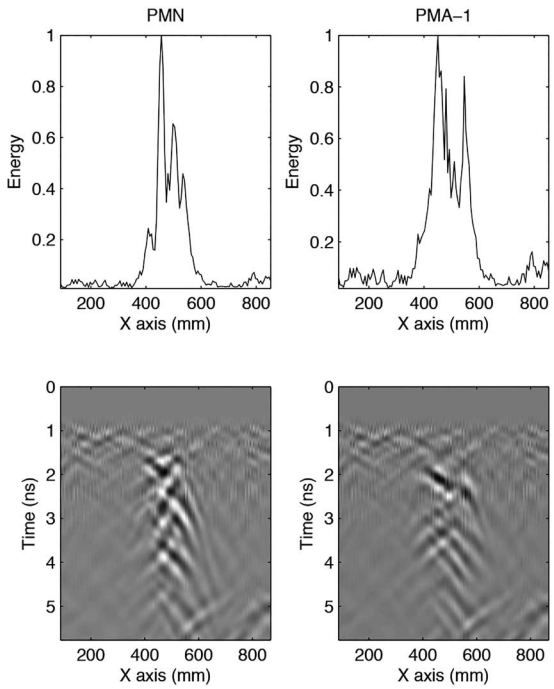


Fig. 20. B-Scans using the 1.5-GHz antenna for the models illustrated in Fig. 19. A quadratic gain and a high pass filter are applied to the raw data.

2.66 g/cm$^3$, $\rho_b = 1.5$ g/cm$^3$, $C = 0.5$, $S = 0.5$, and the water volumetric fraction varies from $m_w = 0$ to 0.25. The model antenna unit used was the 1.5 GHz and it was placed relatively close to the ground. Fig. 20 clearly illustrates the differences between the two B-Scans (a quadratic gain and a high pass filter are applied for both cases). From this, it is clear that a numerical scheme that potentially can be used to provide training sets

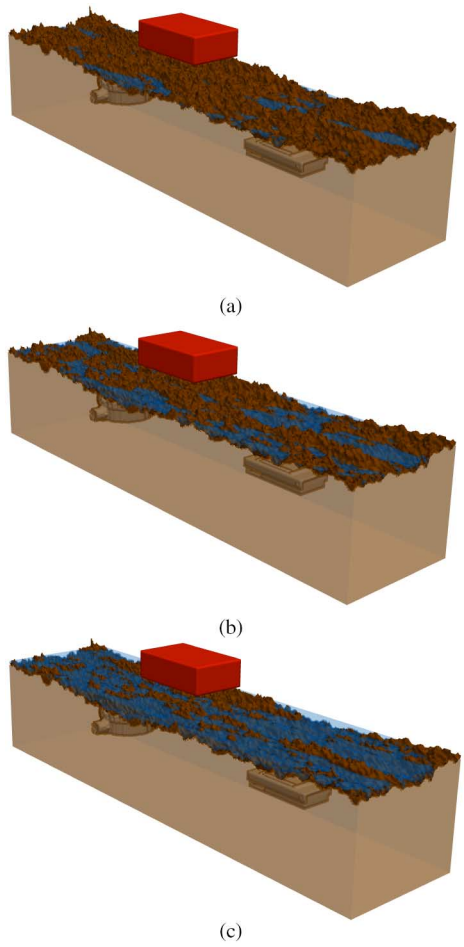


Fig. 21. Water puddles with gradually increasing size over a homogenous saturated sand with fractal rough surface. The soil's properties are $\rho_s = 2.66$ g/cm$^3$, $\rho_b = 2$ g/cm$^3$, $C = 0.5$, $S = 0.5$, and $m_u = 0.15$.

for machine learning should be able to predict the signatures of specific landmines and not generic simplified geometrical objects.

### D. Water Puddles

AP landmines can be found in a variety of environments [10]. Humid environments with saturated soils and water puddles are a common environment in which AP landmines can be found (e.g., Bosnia, Cambodia etc. [10]). In this section, we will briefly examine how water puddles can affect the performance of GPR for AP landmine detection.

The dimensions of the models are $1000 \times 250 \times 450$ mm, the modeled antennas are placed close to the ground surface (40 mm) and the AP landmines are buried at 60 mm depth. The soil is a homogenous saturated sand with $\rho_s = 2.66$ g/cm$^3$, $\rho_b = 2$ g/cm$^3$, $C = 0.5$, $S = 0.5$, and $m_u = 0.15$. Three different scenarios are examined in which water puddles are gradually increased (see Fig. 21). The complex relative electrical permittivity of water is a Debye function (10) with $t_{0,w} = 5.8$ ps, $\epsilon_{w,s} = 80.1$, and $\epsilon_{w,\infty} = 4.9$ [56]. Notice that only the dipolar relaxation of the water is used in the simulations. The conductive term, which is related to the

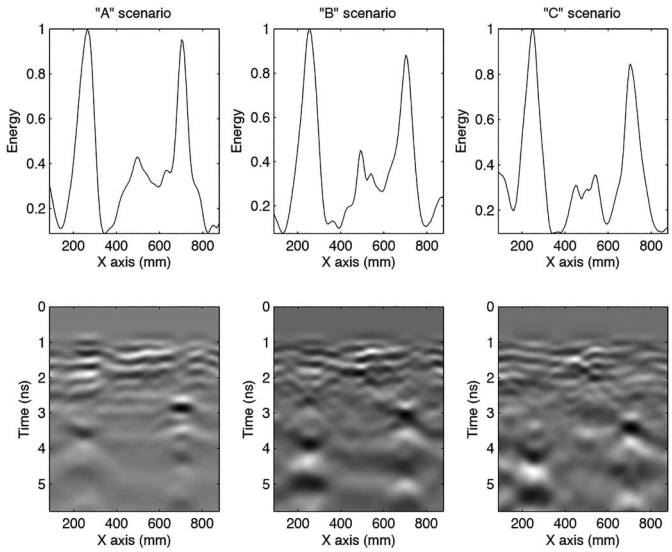


Fig. 22. B-Scans of the models shown in Fig. 21 using the 1.5-GHz antenna. "A," "B," and "C" scenarios correspond to the gradual increase of the water puddles. A quadratic gain and subsequently an average removal technique are applied to the raw data. The $X$-axis corresponds to the center of the antenna unit.

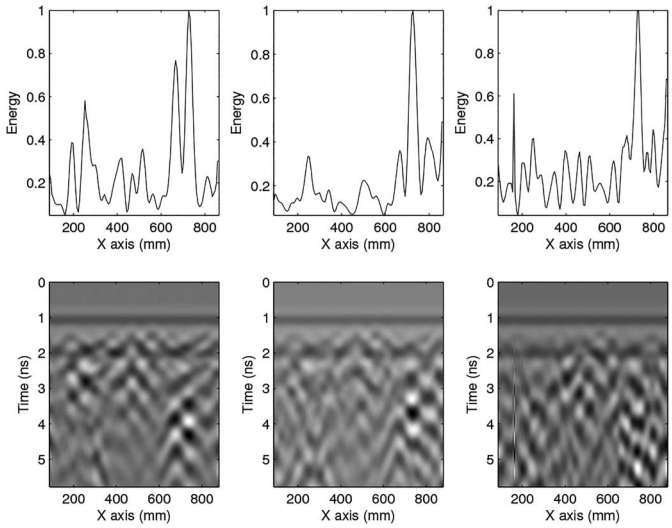


Fig. 23. Similar to Fig. 22 using the 1.2-GHz antenna. Instead of average removal, a high pass filter is applied.

salinity of water [96], is neglected. This is due to the fact that water puddles mostly consist of fresh water for which the main loss mechanism is the dipolar relaxation. If high-salinity water needs to be modeled, the formula suggested by [96] can be used in order to express conductivity with respect to temperature and particles per thousands (ppt). Subsequently, the conductive term can be easily implemented in FDTD. Figs. 22 and 23 illustrate both B-Scans and energy plots using the 1.5- and 1.2-GHz antenna, respectively. A quadratic gain is applied to the resulting B-Scans using both antennas. An average removal technique [92] is proven to give good results for the 1.5 GHz but does not perform equally well when the 1.2-GHz antenna is employed. Due to that, a high pass filter is applied to the B-Scan obtained when using the 1.2-GHz antenna and an average removal is used for the 1.5-GHz antenna. Increasing the size of the water puddles decreases the quality of the results when using the 1.2-GHz antenna (Fig. 23). In "A" and "B" scenario, the PMN is detectable. Increasing the size of the water puddles in "C" scenario makes the detection of PMN difficult and unreliable (Fig. 23). PMA-1, using the 1.2-GHz antenna (for all the three scenarios) results in weak scattering signals (compared to clutter), which are unreliable for interpretation (Fig. 23). The reasons why PMN is easier to be detected compared with PMA-1 are because more water puddles occur above PMA-1 and because PMN is a bigger target, therefore, easier to be resolved by the incident pulse. Due to the high dipolar losses of the water, no multi-interference phenomena neither waveguide effects occur within the water. The high-frequency propagating modes of a thin dielectric slab (like water puddles) are rapidly attenuating due to water's dipolar losses.

From Figs. 22 and 23, it is evident that the 1.5-GHz antenna gives clearer results with respect to the 1.2 GHz one. The reason for that is because the high-frequency content, which is essential in order to get a clear reflection from the AP landmines, which are small targets, is rapidly attenuating inside the water and the saturated sand. The 1.2-GHz antenna has a lower-frequency content, which manages to pass through the water but it cannot resolve well the AP landmines. The already lower high-frequency content of the 1.2-GHz antenna is attenuated inside the water, due to that, the pulse that finally reaches the AP landmines has a rather lower central frequency that makes the AP landmines undetectable. This is the reason why high pass filtering works better than the average removal processing using the 1.2-GHz antenna (i.e., it enhances the high-frequency content of the B-Scan). On the other hand, the 1.5-GHz antenna has a larger amount of high-frequency content that manages to pass through the water and get a clear reflection from the AP landmines. The reduction of the central frequency of the pulse due to the water puddles is illustrated in Fig. 22. In all the scenarios ("A," "B," and "C"), the early reflections from the surface have a higher-frequency content compared with the later reflections from the AP landmines. As the size of the water puddles increases the frequency content of the resulting scattering fields from the AP landmines is decreased. This is also due to the Debye pole which describes the dielectric properties of the saturated sand.

### *E. Water Puddles and Vegetation*

In this last section, we examine how the combination of rough surface, water puddles, and vegetation affects the simulated GPR performance for AP landmine detection. Three different cases are examined in which, rough surface, water puddles, and vegetation are implemented into the models. The dimensions of the model are $1000 \times 250 \times 450$ mm, the properties of the soil are $\rho_s = 2.66\ \mathrm{g/cm^3}$, $\rho_b = 2\ \mathrm{g/cm^3}$, $C = 0.5$, $S = 0.5$, and the water volumetric fraction varies stochastically from $m_u = 0$ to $0.25$. The water weight-based fraction of the vegetation is equal $M = 0.4$. In the first case, the AP landmine PMA-1 is buried in the center of the model at 60 mm depth, in the second case, AP landmine PMN is buried in the center of the model also at 60 mm depth, and in the the

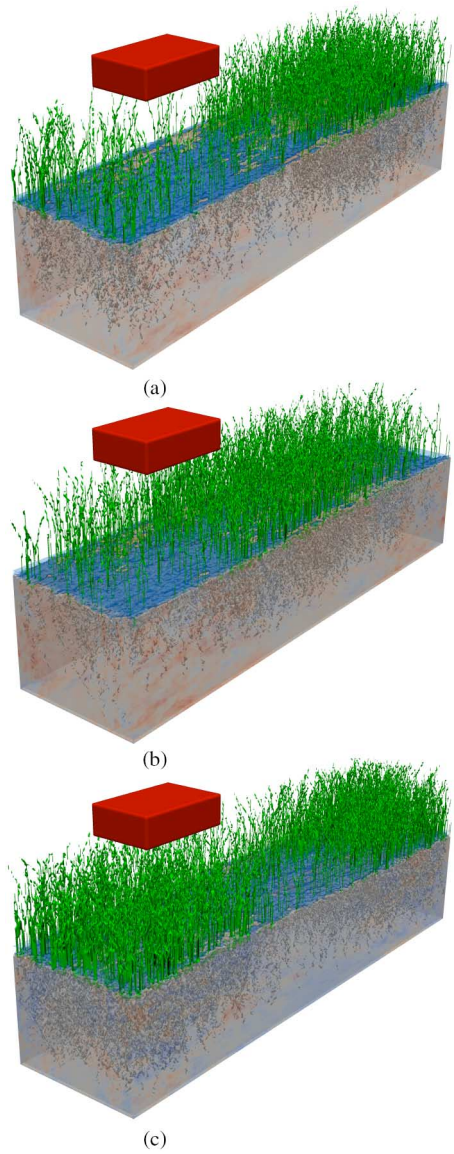


Fig. 24. Three different complex media with a stochastically varied water volumetric fraction, rough surface, water puddles, and vegetation. In case "A," the AP landmine PMA-1 is buried at the center of the model at approximately 60 mm depth, In case "B," PMN is placed 60 mm (approximately) beneath the ground surface. In case "C," no landmines are present.

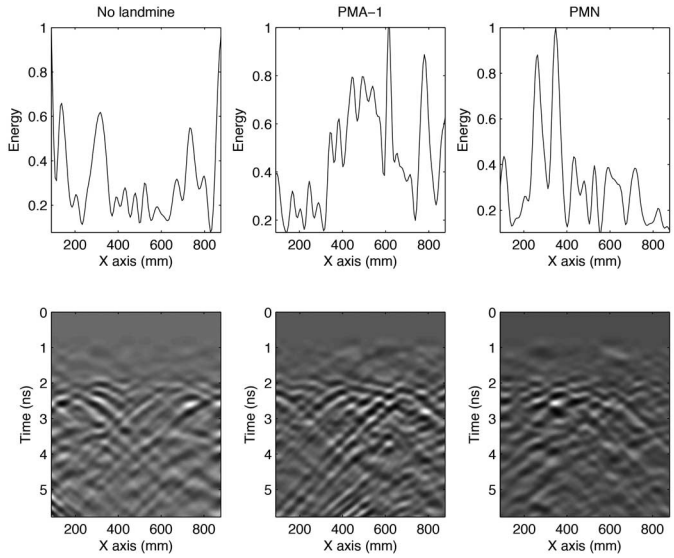


Fig. 25. B-Scans and energy plots using the 1.5-GHz antenna for the cases shown in Fig. 24. A quadratic gain and subsequently a singular value decomposition (four dominant eigenvalues are filtered out) are applied to the raw data. The $X$-axis corresponds to the center of the antenna unit.

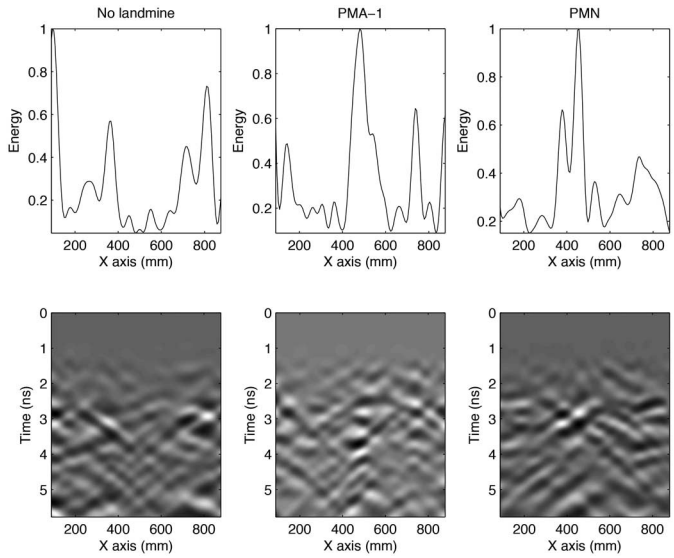


Fig. 26. Same with Fig. 25 using the 1.2-GHz antenna.

third case, no landmines are present in order to investigate the false alarms, which might occur (Fig. 24). One interpretation of these examples is to assume that they do resemble a tropical-humid environment in which AP landmines are frequently found (PMN has been extensively used at the Thai border [88] in heavily vegetated jungle environments). As AP landmines can be found in a wide range of environments, from arid to tropical [9], an efficient numerical scheme should be capable of addressing the issue of diversity and not be constrained to specific cases.

Figs. 25 and 26 illustrate the B-Scans and the energy plots using the 1.5- and 1.2-GHz antenna models, respectively. A quadratic gain and an SVD having four dominant eigenvalues filtered out are applied to the raw data. Using both antenna models results to noisy and difficult to interpret B-scans. The 1.2-GHz antenna gives indications of PMN and PMA-1 but similar patterns also occur in the case of no landmines. This increases the false alarm rate to a level that demining could become more difficult and rather time consuming. Using different processing algorithms (e.g., SVD filtering out different eigenvalues, average removal technique, high pass filter, and adaptive ground removal [94], [95]) leads to equally unreliable results. This clearly illustrates the difficulties that GPR has in some truly complex environments. It is evident from these examples that a numerical scheme that aims to be used as a testbed for developing GPR antennas and advanced processing methods should be capable of producing difficult and challenging data sets. Previous approaches [31]–[37] often resulted in rather clinical B-Scans that were easy to be addressed using trivial processing methods.

## VI. Conclusion

A systematic framework for accurate and realistic numerical modeling of GPR for landmine detection has been introduced. Methods for implementing both the dielectric properties and the geometrical characteristics of the subsurface were proposed as well as methods for implementing vegetation into the models. The effects of vegetation, water puddles, rough surface, and complex soils were examined and cases shown for which GPR—using the specific modeled antennas—has difficulties in clearly and easily detecting the simulated AP landmines. This is in contrast to results from more clinical and simplified models in which numerical GPR modeling gives usually clear and predictable results. Therefore, it appears that realistic simulation results can more consistently predict the GPR's behavior in a manner that is closer to the experience of using GPR in the field.

The overall aim of this work was to investigate the possibility of modeling GPR for landmine detection as much as realistically as possible. The availability of such a detailed numerical modeling framework allows us to investigate in the future advanced processing algorithms and new interpretation schemes without having to oversimplify the problem that often produces predictable outcomes and lead to approaches that as seen in practice do not always perform well in the field. Extensive field testing is obviously the only viable route to be certain that a new approach could be beneficial. However, such a realistic modeling framework is valuable in the phase of developing and testing ideas. Finally, it has also been illustrated via the numerical modeling examples that processing methods are often case sensitive. As a result, interpretation methods must be validated using a diverse set of scenarios. A realistic numerical model is a practical and efficient way to address this issue by providing synthetic but nonetheless realistic data. The long-term intention of this modeling work is to inform and support GPR antenna design, provides a reliable testbed for developing advanced signal processing approaches, and used as a training platform for machine learning purposes.

## References


[1] M. Acheroy, "Mine action: Status of sensor technology for close-in and remote detection of anti-personnel mines," *Near Surf. Geophys.*, vol. 5, pp. 43–55, Feb. 2007.

[2] B. Claudio, G. Bertrand, G. Frederic, P. Pierre-Yves, and C. Olivier, "Ground penetrating radar and imaging metal detector for antipersonnel detection," *J. Appl. Geophys.*, vol. 40, pp. 59–71, Oct. 1998.

[3] M. A. Cameron, R. J. Lawson, and B. W. Tomlin, *To Walk Without Fear: The Global Movement to Ban Landmines*, 1st ed. London, U.K.: Oxford Univ. Press, USA, Dec. 1998.

[4] APOPO. (2006). *A Belgian Research Organisation That Was Initiated in Response to the Global Landmine Problem* [Online]. Available: http://www.apopo.org/. Accessed: Nov. 30, 2014.

[5] C. P. Gooneratne, S. C. Mukhopahyay, and G. S. Gupta, "A review of sensing technologies for landmine detection: Unmanned vehicle based approach," in *Proc. 2nd Int. Conf. Auton. Robots Agents*, Palmerston North, New Zealand, Dec. 2004, pp. 401–407.

[6] C. T. Schroder and W. R. Scott, "A finite-difference model to study the elastic-wave interactions with buried landmines," *IEEE Trans. Geosci. Remote Sens.*, vol. 38, no. 4, pp. 1505–1512, Jul. 2000.

[7] P. Church, J. E. McFee, S. Gagnon, and P. Wort, "Electrical impedance tomographic imaging of buried landmines," *IEEE Trans. Geosci. Remote Sens.*, vol. 44, no. 9, pp. 2407–2420, Sep. 2006.

[8] M. Metwaly, "Detection of metallic and plastic landmines using GPR and 2-D resistivity techniques," *Nat. Hazards Earth Syst. Sci.*, vol. 7, pp. 755–763, Dec. 2007.

[9] D. J. Daniels, *Ground Penetrating Radar*, 2nd ed. London, U.K.: Institution of Engineering and Technology, 2004.

[10] D. J. Daniels, "A review of GPR for landmine detection," *Int. J. Sens. Imag.*, vol. 7, no. 3, pp. 90–123, Dec. 2006.

[11] I. Giannakis, A. Giannopoulos, C. Warren, and N. Davidson, "Numerical modelling and neural networks for landmine detection using ground penetrating radar," in *Proc. Int. Workshop Adv. Ground Penetrat. Radar*, Florence, Italy, 2015, in press.

[12] M. N. O. Sadiku, *Numerical Techniques in Electromagnetics*, 2nd ed. Boca Raton, FL, USA: CRC Press, 2000.

[13] J. Crank and P. Nicolson, "A practical method for numerical evaluation of solutions of partial differential equations of the heat-conduction type," in *Proc. Cambridge Philos. Soc.*, 1947, vol. 43, pp. 50–67.

[14] T. Namiki, "A new FDTD algorithm based on alternating-direction implicit method," *IEEE Trans. Microw. Theory Techn.*, vol. 47, no. 10, pp. 2003–2007, Oct. 1999.

[15] A. Taflove and S. C. Hagness, *Computational Electrodynamics, the Finite-Difference Time-Domain Method*, 2nd ed. Norwood, MA, USA: Artech House, 2000.

[16] K. S. Kunz and R. J. Luebbers, *The Finite-Difference Time-Domain Method for Electromagnetics*. Boca Raton, FL, USA: CRC Press, 1993.

[17] N. J. Cassidy, "A review of practical numerical modelling methods for the advanced interpretation of ground-penetrating radar in near-surface environments," *Near Surf. Geophys.*, vol. 5, pp. 5–21, Feb. 2007.

[18] A. Giannopoulos, "Modeling ground penetrating radar by GprMax," *Constructions and Buildings Materials*, vol. 19, 2005, pp. 755–762.

[19] K. S. Yee, "Numerical solution of initial boundary value problems involving Maxwell's equations in isotropic media," *IEEE Trans. Antennas Propag.*, vol. 14, no. 3, pp. 302–307, May 1966.

[20] V. Wilson, C. Power, A. Giannopoulos, J. Gerhard, and G. Grant, "DNAPL mapping by ground penetrating radar examined via numerical simulation," *J. Appl. Geophys.*, vol. 69, pp. 140–149, Dec. 2009.

[21] J. M. Carcione, "Ground-penetrating radar: Wave theory and numerical simulations in lossy anisotropic media," *Geophysics*, vol. 61, pp. 1664–1677, Dec. 1996.

[22] R. Hu, L. Lu, and S. Wang, "The numerical simulation study on ground penetrating radar detection of the typical adverse geological structure," in *Proc. 14th Int. Conf. Ground Penetrat. Radar (GPR)*, Jun. 2012, pp. 243–247.

[23] C. Ozturk and M. G. Drahor, "Synthetic GPR modelling studies on shallow geological properties and its comparison with the real data," in *Proc. 13th Int. Conf. Ground Penetrat. Radar (GPR)*, Jun. 2010, pp. 1–4.

[24] H. Xianqi, Z. Ziqiang, L. Guangyin, and L. Qunyi, "The FDTD modeling of GPR for tunnel inspection," in *Proc. IEEE Int. Conf. Inf. Eng. Comput. Sci.*, Dec. 2009, pp. 1–4.

[25] N. J. Cassidy and T. M. Millington, "The application of finite-difference time-domain modelling for the assessment of GPR in magnetically lossy materials," *J. Appl. Geophys.*, vol. 67, pp. 296–308, Apr. 2009.

[26] N. Diamanti and A. Giannopoulos, "Employing ADI-FDTD sub-grids for GPR numerical modelling and their application to study ring separation in brick masonry arch bridges," *Near Surf. Geophys.*, vol. 9, pp. 245–256, Jun. 2011.

[27] K. Belli, C.M Rappaport, Z. He, and S. Wadia-Fascetti, "Effectiveness of 2-D and 2.5-D FDTD ground-penetrating radar modeling for bridge-deck deterioration evaluated by 3-D FDTD," *IEEE Trans. Geosci. Remote Sens.*, vol. 47, no. 11, pp. 3656–3663, Nov. 2009.

[28] W. S. Hammon, III, G. A. McMechan, and X. Zeng, "Forensic GOR: Finite-difference simulations of responses from buried human remains," *J. Appl. Geophys.*, vol. 45, pp. 171–186, Oct. 2000.

[29] L. Sixin, W. Junjun, Z. Junfeng, and Z. Zhaofa, "Numerical simulations of borehole radar detection for metal ore," *IEEE Trans. Geosci. Remote Sens.*, vol. 8, no. 2, pp. 308–312, Mar. 2011.

[30] L. Sixin and F. Yanqian, "Airborne GPR: Advances and numerical simulation," in *IEEE Int. Geosci. Remote Sens. Symp.*, Jul. 2011, pp. 3397–3400.

[31] L. Gurel and U. Oguz, "Three-dimensional FDTD modelling of a ground-penetrating radar," *IEEE Trans. Geosci. Remote Sens.*, vol. 38, no. 4, pp. 1513–1521, Jul. 2000.

[32] L. Gurel and U. Oguz, "Simulations of ground-penetrating radars over lossy and heterogeneous grounds," *IEEE Trans. Geosci. Remote Sens.*, vol. 39, no. 6, pp. 1190–1197, Jun. 2001.

[33] U. Oguz and L. Gurel, "Frequency responses of ground-penetrating radars operating over highly lossy grounds," *IEEE Trans. Geosci. Remote Sens.*, vol. 40, no. 6, pp. 1385–1394, Jun. 2002.

[34] L. Gurel and U. Oguz, "Optimization of the transmitter–receiver separation in the ground-penetrating radar," *IEEE Trans. Geosci. Remote Sens.*, vol. 51, no. 3, pp. 362–370, Mar. 2003.

[35] M. A. Gonzalez-Huici, U. Uschkerat, and A. Hoerdt, "Numerical simulation of electromagnetic-wave propagation for land mine detection using GPR," in *Proc. IEEE Int. Geosci. Remote Sens. Symp.*, Jul. 23–28, 2007, pp. 4957–4960.

[36] M. A. Gonzalez-Huici and U. Uschkerat, "GPR modeling for landmine detection," in *Proc. Int. Symp. Electromagn. Theory (EMTS)*, Aug. 2010, pp. 152–155.

[37] M. A. Gonzalez-Huici, "A strategy for landmine detection and recognition using simulated GPR responses," in *Proc. 14th Int. Conf. Ground Penetrat. Radar (GPR)*, Jun. 2012, pp. 871–876.

[38] J. H. Bradform, "Frequency-dependent attenuation analysis of ground-penetrating radar data," *Geophysics*, vol. 72, no. 3, pp. j7–j16, Jun. 2007.

[39] R. J. Sengwa and A. Soni, "Low-frequency dielectric dispersion and microwave dielectric properties of dry and water-saturated limestones of Jodhpur region," *Geophysics*, vol. 71, no. 5, pp. G269–G277, Sep. 2006.

[40] M. R. Taherian, W. E. Kenyon, and K. A. Safinya, "Measurements of dielectric response of water-saturated rocks," *Geophysics*, vol. 55, no. 12, pp. 1530–1541, Dec. 1990.

[41] G. Turner and A. F. Siggins, "Constant Q attenuation of subsurface radar pulses," *Geophysics*, vol. 59, no. 8 pp. 1192–1200, Aug. 1994.

[42] M. Bano, "Constant dielectric losses of ground-penetrating radar waves," *Geophys. J. Int.*, vol. 124, pp. 279–288, Jan. 1996.

[43] M. Bano, "Modelling of GPR waves for lossy media obeying a complex power law of frequency for dielectric permittivity," *Geophys. Prospect.*, vol. 52, pp. 11–26, Jan. 2004.

[44] F. Hollender and S. Tillard, "Modeling ground-penetrating radar wave propagation and reflection with the Jonscher parameterization," *Geophysics*, vol. 63, no. 6, pp. 1933–1942, Dec. 1998.

[45] J. Clegg and M. P. Robinson, "A genetic algorithm used to fit Debye functions to the dielectric properties of tissues," in *Proc. IEEE Congr. Evol. Comput. (CEC)*, Jul. 2010, pp. 1–8.

[46] D. F. Kelley, T. J. Destan, and R. J. Luebbers, "Debye function expansions of complex permittivity using a hybrid particle swarm-least squares optimisation approach," *IEEE Trans. Antennas Propag.*, vol. 55, no. 7, pp. 1999–2005, Jul. 2007.

[47] I. Giannakis, A. Giannopoulos, and N. Davidson, "Incorporating dispersive electrical properties in FDTD GPR models using a general Cole-Cole dispersion function," in *Proc. 14th Int. Conf. Ground Penetrat. Radar (GPR)*, Jun. 2012, pp. 232–236.

[48] F. Torres, P. Vaudon, and B. Jecko, "Application of fractional derivatives to the FDTD modelling of pulse propagation in a Cole–Cole dispersive medium," *Microw. Opt. Technol. Lett.*, vol. 13, no. 5, pp. 300–304, May 1996.

[49] W. H. Weedon and C. M. Rappaport, "A general method for FDTD modelling of wave propagation in arbitrary frequency-dispersive dielectrics," *IEEE Trans. Antennas Propag.*, vol. 45, pp. 401–410, Mar. 1997.

[50] J. M. Carcione and M. A. Schoenberg, "3-D ground-penetrating radar simulation and plane-wave theory in anisotropic media," *Geophysics*, vol. 65, pp. 1527–1541, Oct. 2000.

[51] T. Bergmann, J. O. Robertsson, and K. Holliger, "Finite-difference modelling of electromagnetic wave propagation in dispersive and attenuating media," *Geophysics*, vol. 62, pp. 856–867, Jun. 1998.

[52] T. Xu and G. A. McMechan, "GPR attenuation and its numerical simulation in 2.5 dimensions," *Geophysics*, vol. 62, no. 1, pp. 403–414, Mar. 1997.

[53] F. L. Teixeira, W. C. Chew, M. Straka, M. L. Oristaglio, and T. Wang, "Finite-difference time-domain simulation of ground penetrating radar on dispersive, inhomogeneous, and conductive soils," *IEEE Trans. Geosci. Remote Sens.*, vol. 36, no. 6, pp. 1928–1937, Nov. 1998.

[54] D. Uduwawala, M. Norgren, and P. Fuks, "A complete FDTD simulation of a real GPR antenna system operating above lossy and dispersive grounds," *Prog. Electromagn. Res.*, vol. 50, pp. 209–229, 2005.

[55] G. E. Atteia and K. F. A. Hussein, "Realistic model of dispersive soils using PLRC-FDTD with applications to GPR systems," *Prog. Electromagn. Res.*, vol. 26, pp. 335–359, 2010.

[56] M. C. Dobson, F. T. Ulaby, M. T. Hallikainen, and M. A. El-Rayes, "Microwave dielectric behavior of wet soil—Part II: Dielectric mixing models," *IEEE Trans. Geosci. Remote Sens.*, vol. GRS-23, pp. 35–46, Jan. 1985.

[57] N. R. Peplinski, F. T. Ulaby, and M. C. Dobson, "Dielectric properties of soils in the 0.3–1.3-GHz range," *IEEE Trans. Geosci. Remote Sens.*, vol. 33, no. 3, pp. 803–807, May 1995.

[58] N. R. Peplinski, F. T. Ulaby, and M. C. Dobson, "Corrections to dielectric properties of soils in the 0.3–1.3-GHz range," *IEEE Trans. Geosci. Remote Sens.*, vol. 33, no. 6, p. 1340, Nov. 1995.

[59] A. Giannopoulos and N. Diamanti, "Numerical modelling of ground-penetrating radar response from rough subsurface interfaces," *Near Surf. Geophys.*, vol. 6, pp. 357–369, Dec. 2008.

[60] D. L. Turcotte, "A fractal interpretation of topography and geoid spectra on the Earth, Moon, Venus and Mars," *J. Geophys. Res.*, vol. 92, no. B4, pp. E597–E601, Mar. 1987.

[61] D. L. Turcotte, *Fractals and Chaos in Geology and Geophysics*. Cambridge, U.K.: The Press Syndicate of the Univ. Cambridge, 1992.

[62] R. B. Rezaur, H. Rahardjo, and E. C. Leong, "Spatial and temporal variability of pore-water pressures in residual soil slopes in a tropical climate," *Earth Surf. Process. Landforms*, vol. 27, pp. 317–338, 2002.

[63] Q. F. Yansui Liu and M. Mikami, "Geostatistical analysis of soil moisture variability in grassland," *J. Arid Environ.*, vol. 58, pp. 357–372, 2004.

[64] J. D. Jabro, W. B. Stevens, R. G. Evans, and W. M. Iversen, "Spatial variability and correlation of selected soil properties in the AP horizon of a CRP grassland," *Appl. Eng. Agric.*, vol. 26, pp. 419–428, 2010.

[65] J. Rea and R. Knight, "Geostatistical analysis of ground-penetrating radar data: A means of describing spatial variation in the subsurface," *Water Resour. Res.*, vol. 34, pp. 329–339, Mar. 1998.

[66] N. L. Carlson, "Dielectric constant of vegetation at 8.5 GHz," Electroscience Lab., Ohio State Univ., Columbus, Tech. Rep. 1903-5, Mar. 1967.

[67] H. S. Tan, "Microwave measurements and modelling of the permittivity of tropical vegetation samples," *Appl. Phys.*, vol. 25, pp. 351–355, Jul. 1981.

[68] K. Lee, C. C. Chen, F. L. Teixeira, and K. H. Lee, "Modeling and investigation of a geometrically complex UWB GPR antenna using FDTD," *IEEE Trans. Antennas Propag.*, vol. 52, no. 8, pp. 1983–1991, Aug. 2004.

[69] D. Uduwawala, "Modeling and investigation of planar parabolic dipoles for GPR applications: A comparison with bow-tie using FDTD," *J. Electromagn. Waves Appl.*, vol. 20, pp. 227–236, 2006.

[70] J. R. Bourgeois and G. S. Smith, "A fully three-dimensional simulation of a ground-penetrating radar: FDTD theory compared with experiment," *IEEE Trans. Geosci. Remote Sens.*, vol. 34, no. 1, pp. 36–44, Jan. 1996.

[71] G. Klysz, J. P. Balayssac, S. Laurens, and X. Ferrieres, "Numerical FDTD simulation of the direct wave propagation of a GPR coupled antenna," in *Proc. 10th Int. Conf. Ground Penetrat. Radar (GPR)*, Jun. 2004, vol. 1, pp. 45–48.

[72] D. Caratelli, A. Yarovoy, and L. P. Ligthart, "Accurate FDTD modelling of resistively-loaded bow-tie antennas for GPR applications," in *Proc. IEEE 3rd Eur. Conf. Antennas Propag.*, Mar. 2009, pp. 2115–2118.

[73] J. M. Bourgeois and G. S. Smith, "A complete electromagnetic simulation of a ground penetrating radar for mine detection: Theory and experiment," in *Proc. IEEE Antennas Propag. Soc. Int. Symp.*, Jul. 13–18, 1997, vol. 2, pp. 986–989.

[74] T. P. Montoya and G. S. Smith, "Resistively-loaded Vee antennas for short-pulse ground penetrating radar," *IEEE Antennas Propag. Soc. Int. Symp.*, Jul. 1996 , vol. 3, pp. 2068–2071.

[75] M. McFadden and W.R. Scott, "Numerical modelling of a spiral-antenna GPR system," in *Proc. IEEE Int. Geosci. Remote Sens. Symp.*, Jul. 2009, vol. 2, pp. 109–112.

[76] A. S. Turk, D. A. Sahinkaya, M. Sezgin, and H. Nazli, "Investigation of convenient antenna designs for ultra-wide band GPR systems," in *Proc. 4th Int. Workshop Adv. Ground Penetrat. Radar (GPR)*, Jun. 2007, pp. 192–196.

[77] C. Warren and A. Giannopoulos, "Creating finite-difference time-domain models of commercial ground-penetrating radar antennas using Taguchi's optimisation method," *Geophysics*, vol. 76, no. 2, pp. G37–G47, Apr. 2011.

[78] C. Warren and A. Giannopoulos, "Investigation of the directivity of a commercial ground-penetrating radar antenna using a finite-difference time-domain antenna model," in *Proc. 14th Int. Conf. Ground Penetrat. Radar (GPR)*, Jun. 2012, pp. 226–231.

[79] G. Klysz, X. Ferrieres, J. P. Balayssac, and S. Laurens, "Simulation of direct wave propagation by numerical FDTD for a GPR coupled antenna," *NDT E Int.*, vol. 39, no. 4, pp. 338–347, Jun. 2006.

[80] J. Kennedy and R. C. Eberhart, "Particle swarm optimization," in *Proc. IEEE Int. Conf. Neural Netw.*, Dec. 1995, vol. 4, pp. 1942–1948.

[81] P. A. Burrough, "Fractal dimensions of landscapes and other environmental data," *Nature*, vol. 294, pp. 240–242, Nov. 1981.

[82] D. Hillel, *Environmental Soil Physics*. New York, NJ, USA: Academic Press, 1980.

[83] F. T. Ulaby and R. P. Jedlicka, "Microwave dielectric properties of plant materials," *IEEE Trans. Geosci. Remote Sens.*, vol. GE-22, no. 4, pp. 406-415, Jul. 1984.
[84] M. A. El-Rayes and F. T. Ulaby, "Microwave dielectric spectrum of vegetation-part I: Experimental observations," *IEEE Trans. Geosci. Remote Sens.*, vol. GE-25, no. 5, pp. 541–549, Sep. 1987.
[85] F. T. Ulaby and M. A. El-Rayes, "Microwave dielectric spectrum of vegetation—Part II: Dual-dispersion model," *IEEE Trans. Geosci. Remote Sens.*, vol. GE-25, no. 5, pp. 550–557, Sep. 1987.
[86] B. L. Shrestha, H. C. Wood, and S. Sokhansanj, "Modeling of vegetation permittivity at microwave frequencies," *IEEE Trans. Geosci. Remote Sens.*, vol. 45, no. 2, pp. 342–348, Feb. 2007.
[87] A. Franchois, Y. Pineiro, and R. H. Lang, "Microwave permittivity measurements of two conifers," *IEEE Trans. Geosci. Remote Sens.*, vol. 36, no. 5, pp. 1384–1395, Sep. 1998.
[88] Physicians for Human RIghts, *Landmines, A Deadly Legacy*. Human Rights Watch, New York, NY, USA, 2003.
[89] Reporting formats for Article 7, Convention on the prohibition of the use, stockpiling, production and transfer of anti-personnel mines and on their destruction, The Republic of Croatia, 2014.
[90] J. P. Berenger, "A perfectly matched layer for the absorption of electromagnetic waves," *J. Comput. Phys.*, vol. 114, pp. 185–200, Aug. 1994.
[91] University of Edinburgh. (2014, Nov. 30), *Edinburgh Compute and Data Facility* [Online]. Available: www.ecdf.ed.ac.uk
[92] J. H. Kim, S. J. Cho, and M. J. Yi, "Removal of ringing noise in GPR data by signal processing," *Geosci. J.*, vol. 11, pp. 75–81, Mar. 2007.
[93] K. Takahashi, J. Igel, H. Preetz, and M. Sato, "Influence of heterogeneous soils and clutter on the performance of ground-penetrating radar for landmine detection," *IEEE Trans. Geosci. Remote Sens.*, vol. 52, no. 6, pp. 3464–3472, Jun. 2014.
[94] H. Brunzell, "Detection of shallowly buried objects using impulse radar," *IEEE Trans. Geosci. Remote Sens.*, vol. 37, no. 2, pp. 875–886, Mar. 1999.
[95] R. Wu, A. Clement, J. Li, E. G. Larsson, M. Bradley, J. Habersat, and G. Maksymonko, "Adaptive ground bounce removal," *Electron. Lett.*, vol. 37, no. 20, pp. 1250–1252, Sep. 2001.
[96] A. Stogryn, "Equations for calculating the dielectric constant of saline water," *IEEE Trans. Antennas Propag.*, vol. MTT-19, no. 8, pp. 733–736, Aug. 1971.

**Iraklis Giannakis** received the B.Sc. degree in geology and the M.Sc. degree in geophysics from the Aristotle University of Thessaloniki, Thessaloniki, Greece, in 2009 and 2011, respectively. He is currently pursuing the Ph.D. degree in engineering at the School of Engineering, University of Edinburgh, Edinburgh, U.K.

He is currently working on the numerical modeling of ground penetrating radar and its application to landmine detection. His research interests include development and application of near surface geophysical techniques.

**Antonios Giannopoulos** received the B.Sc. degree in geology from the Aristotle University of Thessaloniki, Thessaloniki, Greece, and the D.Phil. degree in electronics from the University of York, York, U.K., in 1991 and 1997, respectively.

Since 2009, he has been a Senior Lecturer with the School of Engineering, Institute for Infrastructure and Environment, University of Edinburgh, Edinburgh, U.K. He is the author of gprMax (www.gprmax.com), a freely available FDTD GPR simulator. He is a Member of SEG and EAGE. His research interests include advanced numerical modeling of ground penetrating radar, computational electromagnetics and the development and application of geophysical techniques to shallow depth geophysical, and nondestructive testing problems.

**Craig Warren** received the B.E. degree in electrical and mechanical engineering and the Ph.D. degree in engineering from the University of Edinburgh, Edinburgh, U.K., in 2003 and 2009, respectively.

From 2010 to 2013, he held the positions of Teaching Fellow and Learning Technologist, and is currently a Research Associate with the University of Edinburgh. He is a Chartered Engineer (C.Eng.). His research interests include development of numerical models of ground-penetrating radar and novel applications of GPR to engineering problems, engineering education, and technology enhanced learning.

Dr. Warren is a Fellow of the Higher Education Academy (FHEA), U.K., and a member of both the Institution of Mechanical Engineers (IMechE), U.K., and the Institution of Engineering Technology (IET), U.K.